

How Do Enzymes Orient When Trapped on Metal–Organic Framework (MOF) Surfaces?

Yanxiong Pan,[†] Hui Li,[†] Jasmin Farmakes,[†] Feng Xiao,[‡] Bingcan Chen,[§] Shengqian Ma,^{*,||} and Zhongyu Yang^{*,†}

[†]Department of Chemistry and Biochemistry, North Dakota State University, Fargo, North Dakota 58108, United States

[‡]Department of Civil Engineering, University of North Dakota, Grand Forks, North Dakota 58202, United States

[§]Department of Plant Sciences, North Dakota State University, Fargo, North Dakota 58108, United States

^{||}Department of Chemistry and Biochemistry, University of South Florida, Tampa, Florida 33620, United States

Supporting Information

ABSTRACT: Enzyme immobilization in metal–organic frameworks (MOFs) offers retained enzyme integrity and activity, enhanced stability, and reduced leaching. Trapping enzymes on MOF surfaces would allow for catalysis involving large substrates. In both cases, the catalytic efficiency and selectivity depend not only on enzyme integrity/concentration but also orientation. However, it has been a challenge to determine the orientation of enzymes that are supported on solid matrices, which is even more challenging for enzymes immobilized/trapped in MOFs due to the interferences of the MOF background signals. To address such challenge, we demonstrate in this work the utilization of site-directed spin labeling in combination with Electron Paramagnetic Resonance spectroscopy, which allows for the first time the characterization of the orientation of enzymes trapped on MOF surfaces. The obtained insights are fundamentally important for MOF-based enzyme immobilization design and understanding enzyme orientation once trapped in solid matrices or even cellular confinement conditions.

Enzyme immobilization improves biocatalysis, sensing, biofuel, and biomedicine by enhancing enzyme stability and cost-efficiency.^{1–5} Once immobilized, the catalytic efficiency and selectivity of an enzyme depend not only on its integrity/concentration but also on the orientation with respect to the solid surface.^{6–8} Herein a proper orientation can decrease the mass transfer limitation of the substrate and enhance the efficiency/selectivity.^{9–11} Therefore, knowing enzyme orientation is important for not only understanding the catalytic efficiency but also guiding the design of proper platforms for enzyme immobilization.^{12–14} Covalently linking an enzyme to a surface can provide controllable orientation but may encounter enzyme structure/function perturbation due to the chemical modification to the enzyme.^{15,16} Physical adsorption involves less perturbation but faces random enzyme orientation and leaching. Steric trapping may create specific orientation without enzyme chemical modification. In this case, enzyme conformational changes may be needed in order to enter the steric traps.¹⁷

Metal–organic frameworks (MOFs) have recently been demonstrated as advantageous platforms for immobilizing enzymes which overcome most barriers mentioned above.^{18–24} However, enzymes are mainly encapsulated in MOF cages/channels, which prevent catalysis reactions involving large substrates.^{11,25–28} Zeolitic Imidazolate Frameworks (ZIFs) are able to trap enzymes in their crystal defects^{21,22,29–32} including defects on the surface, which may allow for large substrate catalysis. In addition, the enzyme is “loaded” from the inside of the crystal, which does not require enzyme modification or conformational changes. Lastly, enzymes trapped in ZIFs were shown to be functional.^{22,30,31,33} While these promising features solve most of the challenges discussed above, enzyme orientation is still challenging to probe for most protein investigation approaches due to the complexities caused by the ZIF background signals. Lacking such orientation information limits a better understanding of the catalytic behavior of enzymes trapped on ZIFs and design of MOF-based materials for trapping enzymes.^{34–37}

These barriers can be overcome by site-directed spin labeling (SDSL) in combination with Electron Paramagnetic Resonance (EPR) spectroscopy.³⁸ In SDSL, a protein site of interest is mutated to a cysteine, followed by attaching a stable nitroxyl moiety to form a spin label side chain (often known as “R1”).³⁹ Then, EPR’s “penetrating” power reports only the dynamics of the R1 side chain, regardless of the interferences from the background materials.^{38,40–42} SDSL-EPR has been applied to probe structural information on proteins adsorbed to solid surfaces or porous materials.^{41–43} For cysteine-rich proteins, unnatural amino acids can be used to attach the spin label side chain.⁴⁴ In this work, for proof-of-principle, we determined the orientation of a model enzyme, lysozyme, trapped on the surface of ZIF-8 using SDSL-EPR. Lysozyme cleaves the 1,4-glycosidic bond of bacterial cell walls (size of $\sim\mu\text{m}$).^{45,46} Lysozyme is a good model for our purpose because its substrate size is much larger than the pore size of ZIF-8, so any activity from the enzyme/ZIF-8 composites would indicate the presence of active enzymes trapped on the ZIF-8 external surface. Once trapped, the backbone dynamics of lysozyme were probed site-specifically via SDSL-EPR. The regions

Received: August 30, 2018

Published: November 12, 2018



exposed to solvents have increased dynamics compared to those that are buried, which is the principle used to reveal the enzyme orientation on ZIF-8 surfaces. This work represents the first report of orientation and dynamics of an enzyme trapped on MOF surfaces. The structural insights are fundamentally important for MOF-based biomaterials design.

The hen lysozyme (hL)/ZIF-8 composite was prepared as described in the Supporting Information, SI.²² Transmission Electron Microscopy (TEM) images of the cocrystals show that the surface of the hL/ZIF-8 composite in methanol or buffer (Figure 1C and D) is not as smooth as the ZIF-8 alone

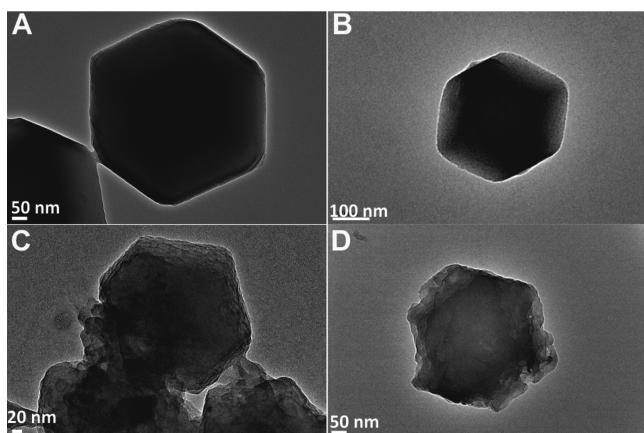


Figure 1. TEM images of ZIF-8 in MeOH (A) and PBS buffer (B) and hL/ZIF-8 composites in MeOH (C) and PBS buffer (D).

(Figure 1A and B), consistent with a previous report.²² Powder X-ray Diffraction (PXRD) analysis (Figure 2A) shows that the incorporation of hL did not cause major changes in the crystal scaffold.

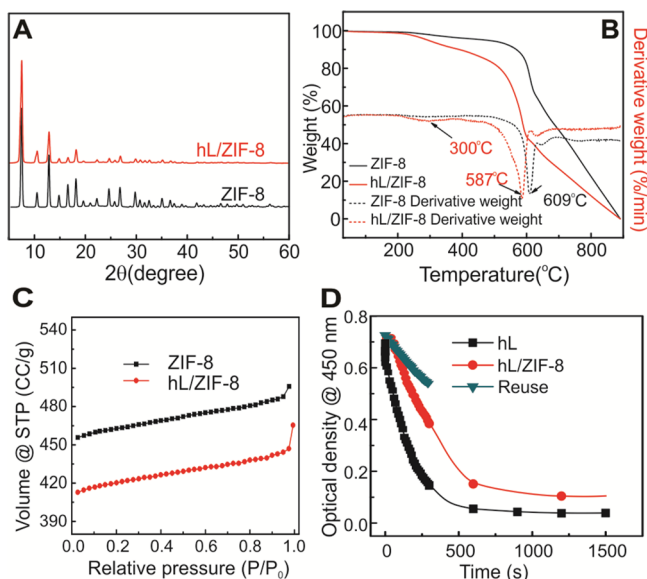


Figure 2. (A) PXRD data of ZIF-8 (black) and hL/ZIF-8 composite (red). (B) TGA data of ZIF-8 (black) and hL/ZIF-8 composite (red) confirm the encapsulation of enzyme. (C) Nitrogen adsorption experiments of ZIF-8 (black) and hL/ZIF-8 composite (red). (D) Activity assay of hL (black squares), hL/ZIF-8 composite (red dots), and hL/ZIF-8 composite after one round of catalysis (green triangles).

Thermal gravimetric analysis (TGA) shows an $\sim 8.7\%$ weight loss (Figure 2B, 215 to 400 °C) consistent with the loss of hL. ZIF-8, hL/ZIF-8, and polyvinylpyrrolidone (PVP) degradation are also present (Figure 2B, 587 and 609 °C peaks are due to hL/ZIF-8 and ZIF-8 degradation, respectively, and the ~ 420 °C peak is due to PVP degradation).⁴⁷ hL reduced the stability of the ZIF-8 which lowers the decomposition temperature. Nitrogen absorption experiments indicate a decrease in the porosity of the crystal upon hL trapping (Figure 2C and SI).

Lysozyme activity test was done by monitoring the optical density of bacterial cell wall at 450 nm (OD450).⁴² Upon confirming no change in OD450 was caused by ZIF-8 alone (Figure S1), we observed a substantial decay of OD450 (Figure 2D red dots) from hL/ZIF-8. The decay rate is slower than that of hL in buffer (Figure 2D black squares) under the same conditions, indicating hL trapped on ZIF-8 is only partially active. This is reasonable because the protein could be both buried inside and trapped on the surface of ZIF-8. Also, after one round of catalytic reaction (~ 2 h; see the SI), the remaining hL/ZIF-8 was still catalytically active, indicating the reusability of hL/ZIF-8 (Figure 2D green triangles).

Next, we proceeded to probe the orientation of the trapped enzyme (principle *vide supra*). In doing so, we utilized the same synthetic procedure to incorporate recombinant T4 phage lysozyme (T4L). We created 6 cysteine mutants, one at a time, scanning most regions of the enzyme (Figure 3A; activity test see the SI). Then, we confirmed that T4L/ZIF-8 cocrystals showed similar properties as hL/ZIF-8.

To probe the backbone dynamics of each labeled site, we employed continuous wave (CW) EPR in PBS buffer (Figure 3 blue traces). For all sites, CW EPR results show first derivative spectra with the low-, mid-, and high-field regions (due to the hyperfine splitting). Within each region, we observe an immobile and a mobile component as indicated by “im” and “m” of the low-field region (example simulations see Figure 3B). In general, a CW EPR spectral component depends on three motions: protein rotational tumbling, backbone dynamics, and the intrinsic motion of R1.³⁸ When protein rotational tumbling is restricted (with no other interactions⁴⁸), the resultant spectra are shown in Figure 3C–G (dotted curves). Furthermore, if the labeled site is in contact with some species (ca. ZIF scaffolds), the spectrum becomes even broader (see the populated “im” peak of blue curves in Figure 3C–G). Essentially, we observed two components for all sites on ZIF-8. For each site, both buried and surface enzymes were detected. Buried enzymes contribute the immobile spectral component due to their highly restricted motion (Figure S6A). For surface enzymes, if the labeled site is buried below the crystal surface (Figure S6C), then it will also contribute an immobile spectral component. A solvent-exposable site (Figure S6B) will result in a mobile component. This is the basis of the two observed spectral components for all sites. Control experiments on enzyme in buffer (Figure 3 green curves) confirm that the selected sites are not intrinsically immobilized.

To quantify the relative population of the two components, we carried out spectral simulations.⁴⁹ In brief, parameters related to the rate and spatial restriction (order) of R1 motion were varied to generate a CW EPR spectrum until a reasonable fit was reached (details see the SI). Our rate and order parameters from the simulation (see Tables S2–S7) indicate that for all sites the immobile component is originated from a highly ordered, slow motion, consistent with R1 in contact

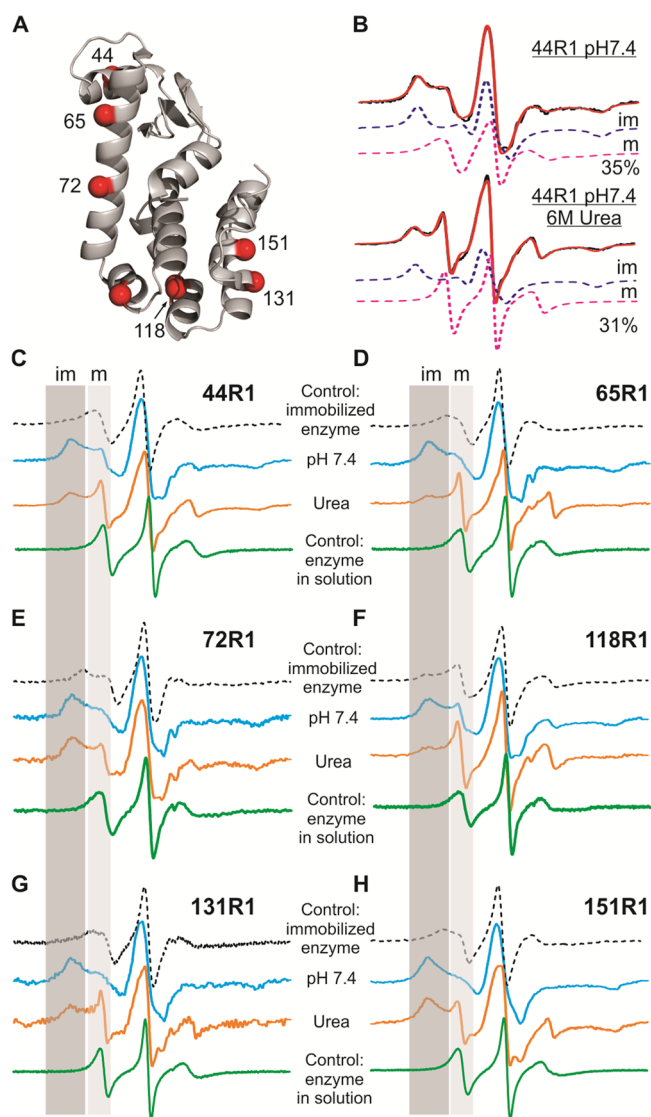


Figure 3. (A) Surface sites of T4L spin labeled with R1. (B) Example spectral simulations of the mobile and immobile components of a labeled site under two conditions. (C–G) CW EPR spectra of six labeled sites under various conditions. The x -axis of each spectrum is 3300–3400 G.

with ZIF-8. The mobile component shows relatively low order and fast motion, consistent with R1 exposed to the solvent. The relative population of the mobile component varies between 12% and 40% depending on labeled sites (Table S8).

To confirm the “m” components are from exposed residues, we employed urea (6 M), which does not influence enzymes encapsulated inside of ZIF-8,²¹ to unfold the surface portion of the protein. For all sites we observe an increase in the density of the “m” peak (Figure 3C–G orange traces), consistent with disordered protein backbones due to local enzyme unfolding. A careful spectral simulation shows reasonable agreement in the mobile component population of each site in the absence and presence of urea (Table S8). The rate parameters of the mobile component for each labeled site (see $R_{z,m}$ in Tables S2–S7) also confirm the increase in the mobility. Furthermore, these data confirmed that different labeled sites have different tendencies to be exposed to the solvent. For example, 131R1 and 151R1 near the C-terminus show less mobile populations than other sites, indicating these regions are less likely exposed

to the solvent. This is consistent with that more aromatic residues exist near the C-terminus (Figure 4 blue stick models

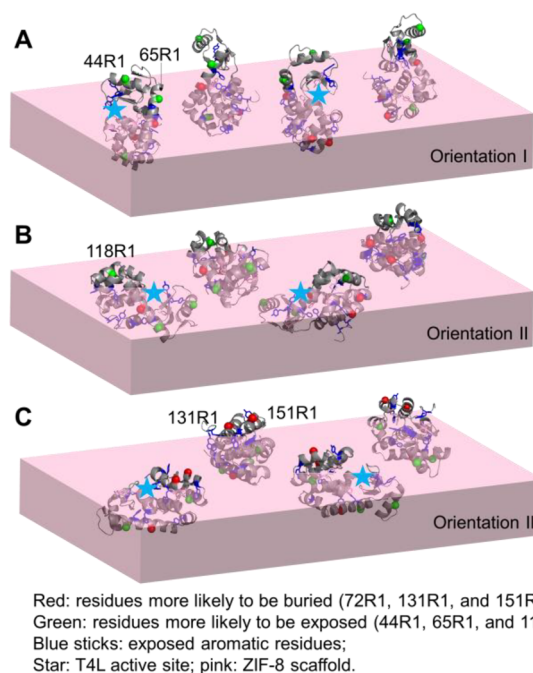


Figure 4. Proposed orientations of T4L on ZIF-8 crystal surface from four angles differing by 90° clockwise. For details of model construction and other possible orientations, see the SI.

and Figure S10) which tend to form more π – π stacking interactions with ZIF-8 imidazole rings and bury the nearby regions. Based on this finding (Table S8), we propose a possible orientation preference of T4L on ZIF-8 surfaces wherein the N-terminus (44R1 and 65R1; Figure 4A green dots) tends to be exposed more to the solvent (orientation I), while the C-terminus (131R1 and 151R1; Figure 4C red dots) tends to be buried in ZIF (orientation III). An interesting site is 118R1 which also tends to be exposed to the solvent (Figure 4B orientation II). A careful look at the structure indicates that this orientation tends to bury more aromatic residues as well. The metals in the ZIF-8 network (Zn^{2+}) may also contribute to the trapping of enzymes in the crystal. However, since the Zn^{2+} binding residues are relatively uniformly distributed through the protein (Figure S11 and associated analysis), it is less likely for metal–residue interactions to contribute to the orientation preference. The dominant factors of the orientation preference are the steric hindrance and the π – π stacking interactions. Orientations II and III (Figure 4B and C) are likely responsible for the activity since these orientations place the active site (Figure 4 stars) toward the solvent/substrates. Orientation I likely suffers from hindrance for substrate access and is less likely responsible for the activity although it has a higher preference.

In conclusion, we demonstrated that enzymes can be sterically trapped on the surface of ZIF-8 crystals. The formed composites were stable under physical perturbation and reusable. The backbone dynamics of enzymes trapped on the ZIF surface can be determined site specifically via SDSL-EPR in combination with spectral analysis, which revealed the tendency of different regions that can be exposed to the solvent. This information was used to depict the orientation preference of T4L on the ZIF-8 surface. In comparison to EPR

relaxation methods for solvent accessibility measurements,⁵⁰ our line shape analysis does not require the addition of paramagnetic agents which simplifies the procedure and avoids potential interactions between the ZIF-8 network and the agents. The obtained orientation will guide our ongoing research on optimizing the building blocks in order to tune the orientation of enzymes on ZIF surfaces. Being able to control enzyme orientation on the MOF surface may offer an opportunity to enable substrate selectivity based on substrate size and/or affinity to MOFs. For example, an orientation facing the active site away from solvent bulk can select small substrates over large ones (Figure S13A), while partially blocking the active site can help distinguish small substrates with different sizes (Figure S13B). For small substrates with different affinities to ZIF/MOF surfaces, it is also possible to select substrates via tuning orientation (Figure S13C). Of course, an orientation facing the active site directly to the solvents is good for large substrate catalysis (Figure S13D). This effort is fundamentally important for MOF-based biomaterials designs for biocatalysis, targeted enzyme delivery, biofuel, and biosensing. The method presented here is applicable to probe enzyme orientation once trapped in cellular confinement conditions.

■ ASSOCIATED CONTENT

Supporting Information

The Supporting Information is available free of charge on the ACS Publications website at DOI: 10.1021/jacs.8b09257.

Enzyme/ZIF-8 composites preparation; basic composite characterization including TEM, PXRD, TGA, N₂ absorption experiments, Zeta-potential measurements; lysozyme activity; T4L expression, purification, and spin labeling procedures; spin labeled T4L secondary structure and activity determination; CW EPR instrument and spectral simulation; urea unfolding kinetics (PDF)

■ AUTHOR INFORMATION

Corresponding Authors

*zhongyu.yang@ndsu.edu

*sqma@usf.edu

ORCID

Feng Xiao: 0000-0001-5686-6055

Bingcan Chen: 0000-0002-4989-547X

Shengqian Ma: 0000-0002-1897-7069

Zhongyu Yang: 0000-0002-3018-3608

Notes

The authors declare no competing financial interest.

■ ACKNOWLEDGMENTS

This work is supported by the New Faculty Startup Funds from the North Dakota State University (Z.Y.). Partial support from the NSF (DMR-1352065) is also acknowledged (S.M.). We appreciate Prof. Hubbell for generously providing the EPR spectral simulation package and Dr. Angel Ugrinov for helping on PXRD data acquisition and analysis.

■ REFERENCES

- (1) Zakharchenko, A.; Guz, N.; Laradji, A. M.; Katz, E.; Minko, S. *Nat. Catal.* **2018**, *1*, 73.
- (2) Wong, L. S.; Khan, F.; Micklefield, J. *Chem. Rev.* **2009**, *109*, 4025.
- (3) Bommarius, A. S.; Paye, M. F. *Chem. Soc. Rev.* **2013**, *42*, 6534.
- (4) Secundo, F. *Chem. Soc. Rev.* **2013**, *42*, 6250.
- (5) Howarth, A. J.; Liu, Y.; Li, P.; Li, Z.; Wang, T. C.; Hupp, J. T.; Farha, O. K. *Nat. Rev. Mater.* **2016**, *1*, 15018.
- (6) Kuchler, A.; Yoshimoto, M.; Luginbühl, S.; Mavelli, F.; Walde, P. *Nat. Nanotechnol.* **2016**, *11*, 409.
- (7) Fu, J.; Yang, Y. R.; Johnson-Buck, A.; Liu, M.; Liu, Y.; Walter, N. G.; Woodbury, N. W.; Yan, H. *Nat. Nanotechnol.* **2014**, *9*, 531.
- (8) Zhang, Y.; Ge, J.; Liu, Z. *ACS Catal.* **2015**, *5*, 4503.
- (9) Shang, W.; Nuffer, J. H.; Dordick, J. S.; Siegel, R. W. *Nano Lett.* **2007**, *7*, 1991.
- (10) Palla, K. S.; Hurlburt, T. J.; Buyanin, A. M.; Somorjai, G. A.; Francis, M. B. *J. Am. Chem. Soc.* **2017**, *139*, 1967.
- (11) Sun, Q.; Fu, C.-W.; Aguila, B.; Perman, J.; Wang, S.; Huang, H.-Y.; Xiao, F.-S.; Ma, S. *J. Am. Chem. Soc.* **2018**, *140*, 984.
- (12) Yang, L.; Gomez-Casado, A.; Young, J. F.; Nguyen, H. D.; Cabanas-Dañés, J.; Huskens, J.; Brunsveld, L.; Jonkheijm, P. *J. Am. Chem. Soc.* **2012**, *134*, 19199.
- (13) Ding, S.; Cargill, A. A.; Medintz, I. L.; Claussen, J. C. *Curr. Opin. Biotechnol.* **2015**, *34*, 242.
- (14) Rodrigues, R. C.; Ortiz, C.; Berenguer-Murcia, A.; Torres, R.; Fernandez-Lafuente, R. *Chem. Soc. Rev.* **2013**, *42*, 6290.
- (15) Hong, R.; Emrick, T.; Rotello, V. M. *J. Am. Chem. Soc.* **2004**, *126*, 13572.
- (16) Hu, Y.; Cheng, H.; Zhao, X.; Wu, J.; Muhammad, F.; Lin, S.; He, J.; Zhou, L.; Zhang, C.; Deng, Y.; Wang, P.; Zhou, Z.; Nie, S.; Wei, H. *ACS Nano* **2017**, *11*, 5558.
- (17) Chen, Y.; Lykourinou, V.; Vetromile, C.; Hoang, T.; Ming, L. J.; Larsen, R. W.; Ma, S. *J. Am. Chem. Soc.* **2012**, *134*, 13188.
- (18) Liang, K.; Coghan, C. J.; Bell, S. G.; Doonan, C.; Falcaro, P. *Chem. Commun.* **2016**, *52*, 473.
- (19) Li, P.; Moon, S.-Y.; Guelta, M. A.; Harvey, S. P.; Hupp, J. T.; Farha, O. K. *J. Am. Chem. Soc.* **2016**, *138*, 8052.
- (20) Li, P.; Moon, S.-Y.; Guelta, M. A.; Lin, L.; Gómez-Gualdrón, D. A.; Snurr, R. Q.; Harvey, S. P.; Hupp, J. T.; Farha, O. K. *ACS Nano* **2016**, *10*, 9174.
- (21) Liao, F. S.; Lo, W. S.; Hsu, Y. S.; Wu, C. C.; Wang, S. C.; Shieh, F. K.; Morabito, J. V.; Chou, L. Y.; Wu, K. C. W.; Tsung, C. K. *J. Am. Chem. Soc.* **2017**, *139*, 6530.
- (22) Lyu, F.; Zhang, Y.; Zare, R. N.; Ge, J.; Liu, Z. *Nano Lett.* **2014**, *14*, 5761.
- (23) Lu, G.; Li, S.; Guo, Z.; Farha, O. K.; Hauser, B. G.; Qi, X.; Wang, Y.; Wang, X.; Han, S.; Liu, X.; DuChene, J. S.; Zhang, H.; Zhang, Q.; Chen, X.; Ma, J.; Loo, S. C. J.; Wei, W. D.; Yang, Y.; Hupp, J. T.; Huo, F. *Nat. Chem.* **2012**, *4*, 310.
- (24) Liang, K.; Richardson, J. J.; Doonan, C. J.; Mulet, X.; Ju, Y.; Cui, J.; Caruso, F.; Falcaro, P. *Angew. Chem., Int. Ed.* **2017**, *56*, 8510.
- (25) Li, P.; Chen, Q.; Wang, T. C.; Vermeulen, N. A.; Mehdi, B. L.; Dohnalkova, A.; Browning, N. D.; Shen, D.; Anderson, R.; Gómez-Gualdrón, D. A.; Cetin, F. M.; Jagiello, J.; Asiri, A. M.; Stoddart, J. F.; Farha, O. K. *Chem.* **2018**, *4*, 1022.
- (26) Lian, X.; Erazo-Oliveras, A.; Pellois, J.-P.; Zhou, H.-C. *Nat. Commun.* **2017**, *8*, 2075.
- (27) Yuan, S.; Zou, L.; Qin, J.-S.; Li, J.; Huang, L.; Feng, L.; Wang, X.; Bosch, M.; Alsalmé, A.; Cagin, T.; Zhou, H.-C. *Nat. Commun.* **2017**, *8*, 15356.
- (28) Li, P.; Modica, J. A.; Howarth, A. J.; Vargas, L. E.; Moghadam, P. Z.; Snurr, R. Q.; Mrksich, M.; Hupp, J. T.; Farha, O. K. *Chem.* **2016**, *1*, 154.
- (29) Wang, Q.; Zhang, X.; Huang, L.; Zhang, Z.; Dong, S. *Angew. Chem., Int. Ed.* **2017**, *56*, 16082.
- (30) Pitzalis, F.; Carucci, C.; Naseri, M.; Fotouhi, L.; Magner, E.; Salis, A. *ChemCatChem* **2018**, *10*, 1478.
- (31) Liang, K.; Ricco, R.; Doherty, C. M.; Styles, M. J.; Bell, S.; Kirby, N.; Mudie, S.; Haylock, D.; Hill, A. J.; Doonan, C. J.; Falcaro, P. *Nat. Commun.* **2015**, *6*, 1.

- (32) Shieh, F. K.; Wang, S. C.; Yen, C. I.; Wu, C. C.; Dutta, S.; Chou, L. Y.; Morabito, J. V.; Hu, P.; Hsu, M. H.; Wu, K. C. W.; Tsung, C. K. *J. Am. Chem. Soc.* **2015**, *137*, 4276.
- (33) Liang, W.; Ricco, R.; Maddigan, N. K.; Dickinson, R. P.; Xu, H.; Li, Q.; Sumbly, C. J.; Bell, S. G.; Falcaro, P.; Doonan, C. J. *Chem. Mater.* **2018**, *30*, 1069.
- (34) Lian, X.; Fang, Y.; Joseph, E.; Wang, Q.; Li, J.; Banerjee, S.; Lollar, C.; Wang, X.; Zhou, H.-C. *Chem. Soc. Rev.* **2017**, *46*, 3386.
- (35) Majewski, M. B.; Howarth, A. J.; Li, P.; Wasielewski, M. R.; Hupp, J. T.; Farha, O. K. *CrystEngComm* **2017**, *19*, 4082.
- (36) Gkaniatsou, E.; Sicard, C. m.; Ricoux, R. m.; Mahy, J.-P.; Steunou, N.; Serre, C. *Mater. Horiz.* **2017**, *4*, 55.
- (37) Doonan, C.; Riccò, R.; Liang, K.; Bradshaw, D.; Falcaro, P. *Acc. Chem. Res.* **2017**, *50*, 1423.
- (38) Hubbell, W. L.; López, C. J.; Altenbach, C.; Yang, Z. *Curr. Opin. Struct. Biol.* **2013**, *23*, 725.
- (39) Fleissner, M. R.; Bridges, M. D.; Brooks, E. K.; Cascio, D.; Kálai, T.; Hideg, K.; Hubbell, W. L. *Proc. Natl. Acad. Sci. U. S. A.* **2011**, *108*, 16241.
- (40) Fanucci, G. E.; Cafiso, D. S. *Curr. Opin. Struct. Biol.* **2006**, *16*, 644.
- (41) Pan, Y.; Neupane, S.; Farmakes, J.; Bridges, M.; Froberg, J.; Rao, J.; Qian, S. Y.; Liu, G.; Choi, Y.; Yang, Z. *Nanoscale* **2017**, *9*, 3512.
- (42) Neupane, S.; Pan, Y.; Li, H.; Patnode, K.; Farmakes, J.; Liu, G.; Yang, Z. *ACS Appl. Nano Mater.* **2018**, *1*, 4053.
- (43) Huang, Y.-W.; Lai, Y.-C.; Tsai, C.-J.; Chiang, Y.-W. *Proc. Natl. Acad. Sci. U. S. A.* **2011**, *108*, 14145–14150.
- (44) Fleissner, M. R.; Brustad, E. M.; Kálai, T.; Altenbach, C.; Cascio, D.; Peters, F. B.; Hideg, K.; Peuker, S.; Schultz, P. G.; Hubbell, W. L. *Proc. Natl. Acad. Sci. U. S. A.* **2009**, *106*, 21637–21642.
- (45) Kuroki, R.; Weaver, L. H.; Matthews, B. W. *Nat. Struct. Mol. Biol.* **1995**, *2*, 1007.
- (46) Mushegian, A. R.; Fullner, K. J.; Koonin, E. V.; Nester, E. W. *Proc. Natl. Acad. Sci. U. S. A.* **1996**, *93*, 7321.
- (47) Choi, S.-J.; Choi, C.; Kim, S.-J.; Cho, H.-J.; Hakim, M.; Jeon, S.; Kim, I.-D. *Sci. Rep.* **2015**, *5*, 8067.
- (48) Yang, Z.; Liu, Y.; Borbat, P.; Zweier, J. L.; Freed, J. H.; Hubbell, W. L. *J. Am. Chem. Soc.* **2012**, *134*, 9950.
- (49) Budil, D. E.; Lee, S.; Saxena, S.; Freed, J. H. *J. Magn. Reson., Ser. A* **1996**, *120*, 155.
- (50) Bridges, M.; Hideg, K.; Hubbell, W. *Appl. Magn. Reson.* **2010**, *37*, 363–390.